PHOTONICS Research

103 GHz germanium-on-silicon photodiode enabled by an optimized U-shaped electrode

Yang Shi,[1,†] Xiang Li,[2,†] Mingjie Zou,[1] Yu Yu,[1,3,5] and Xinliang Zhang[1,3,4,6]

[1]Wuhan National Laboratory for Optoelectronics & School of Optical and Electronic Information, Huazhong University of Science and Technology, Wuhan 430074, China
[2]School of Mechanical Engineering and Electronic Information, China University of Geosciences, Wuhan 430074, China
[3]Optics Valley Laboratory, Wuhan 430074, China
[4]Xidian University, Xi'an 710126, China
[5]e-mail: yuyu@mail.hust.edu.cn
[6]e-mail: xlzhang@mail.hust.edu.cn
[†]These authors contributed equally to this work.

Received 18 May 2023; revised 19 September 2023; accepted 17 October 2023; posted 18 October 2023 (Doc. ID 495958); published 8 December 2023

High-performance germanium photodiodes are crucial components in silicon photonic integrated circuits for large-capacity data communication. However, the bandwidths of most germanium photodiodes are limited by the intractable resistance–capacitance parasitic effect. Here, we introduce a unique U-shaped electrode to alleviate this issue, reducing the parasitic effect by 36% without compromising any other performance. Experimentally, a large bandwidth of 103 GHz, an optical responsivity of 0.95 A/W at 1550 nm, and a dark current as low as 1.3 nA are achieved, leading to a record high specific detectivity. This is the first breakthrough to 100 GHz bandwidth among all vertical germanium photodiodes, to the best of our knowledge. Open eye diagrams of 120 Gb/s on-off keying and 200 Gb/s four-level pulse amplitude signals are well received. This work provides a promising solution for chip-based ultra-fast photodetection. © 2023 Chinese Laser Press

https://doi.org/10.1364/PRJ.495958

1. INTRODUCTION

In the past decade, silicon photonics has made great advances and is widely used in optical communication [1], high-performance computing [2], and quantum signal processing [3]. Due to the complementary metal-oxide-semiconductor (CMOS)-compatible fabrication and feasibility of monolithic integration with microelectronic devices, silicon photonic integrated circuit (SiPIC) is promising to significantly reduce cost and power consumption while increasing integration density [4,5]. Waveguide-integrated germanium (Ge) photodiodes (PDs), being responsible for converting optical signals into electrical form, are key elements in the SiPICs. With the explosive growth of global communication capacity, waveguide PDs with bandwidth surpassing 100 GHz have become a subject of intense research for several decades [6,7]. Among all materials, mainly indium phosphide (InP) or graphene-based PDs enable this goal, owing to the very high carrier mobility [8–11]. Several Ge PDs with >110 GHz bandwidth have been reported thanks to the very narrow intrinsic Ge regions and the reduced carrier transit time [12,13]. Recently, devices with narrow Ge fin sandwiched between *in situ*-doped silicon layers were reported with a bandwidth of 265 GHz [14]. However, the optical responsivities and dark current were compromised due to the narrow intrinsic regions.

Typically, the ultimate bandwidth of a Ge PD is determined by the carrier transit time, and an intrinsic region of 300–400 nm corresponds to a bandwidth of 100 GHz [15]. Although such an intrinsic region is routinely utilized, the practical bandwidth is much below the desired value, primarily limited by the resistance–capacitance parasitic effect. To address this issue, the gain-peaking technology has been proposed to partly offset parasitic capacitance [16–18]. Previous work has further demonstrated that reducing series resistance and matching it with a proper on-electrode inductance can boost the bandwidth, enabling an 80 GHz bandwidth [19]. Nevertheless, in conventional waveguide Ge PDs, shrinking series resistance is limited by the design trade-off with junction capacitance. Typically, the metal electrodes in these devices are parallel to the Ge film (denoted as parallel electrode). As a result, Ge length affects the carrier collection path and thus the cross-section area of the series resistance. This means that reducing series resistance by increasing Ge length in turn increases the junction capacitance, keeping the resistance–capacitance product unchanged.

Here, we demonstrate a high-speed waveguide Ge PD using a specifically designed U-shaped electrode. By establishing an extra carrier collection path to extend the resistance area, the series resistance is lowered by 36% without increasing junction capacitance. On this base, an optimal on-chip inductance is further introduced to partly offset parasitic capacitance. Experimentally, the bandwidth is improved from 83 to 103 GHz, compared with the parallel electrode (also with an optimal inductance). To the best of our knowledge, this is the first vertical Ge PD with a bandwidth greater than 100 GHz. Under the voltage of −1 V, the measured optical responsivity at 1550 nm is 0.95 A/W and the dark current is as low as 1.3 nA, resulting in a record high specific detectivity of 2.95×10^{10} cm·Hz$^{1/2}$·W^{-1}. Open eye diagrams of 120 Gb/s on-off keying (OOK) and 200 Gb/s four-level pulse amplitude (PAM4) signals are obtained for high-speed demonstration. This work provides design guidance for high-speed optoelectronic devices and paves the way for ultra-fast optical interconnects.

2. OPERATION PRINCIPLE AND DEVICE DESIGN

The structural schematic of the proposed waveguide Ge PD with the U-shaped electrode and the equivalent circuit are shown in Fig. 1(a). The active region is a vertical n-i-p junction consisting of 50 nm N^{++} Ge, 350 nm intrinsic Ge (i-Ge), and P^{++} silicon. The 350 nm intrinsic region corresponds to a carrier transit time-determined bandwidth of 120 GHz. Being different from conventional waveguide PDs, the specifically designed U-shaped electrode increases the resistance area and reduces the series resistance without increasing the capacitance. The capacitance is further mitigated by an optimal on-electrode inductance, provided by the metal connection between the PD and pad.

The junction parasitic parameter consists of the series resistance R_S and junction capacitance C_j. Unfortunately, there is a design trade-off between them under parallel electrode [Fig. 1(b)]. Specifically, C_j is from an analogous plate capacitor

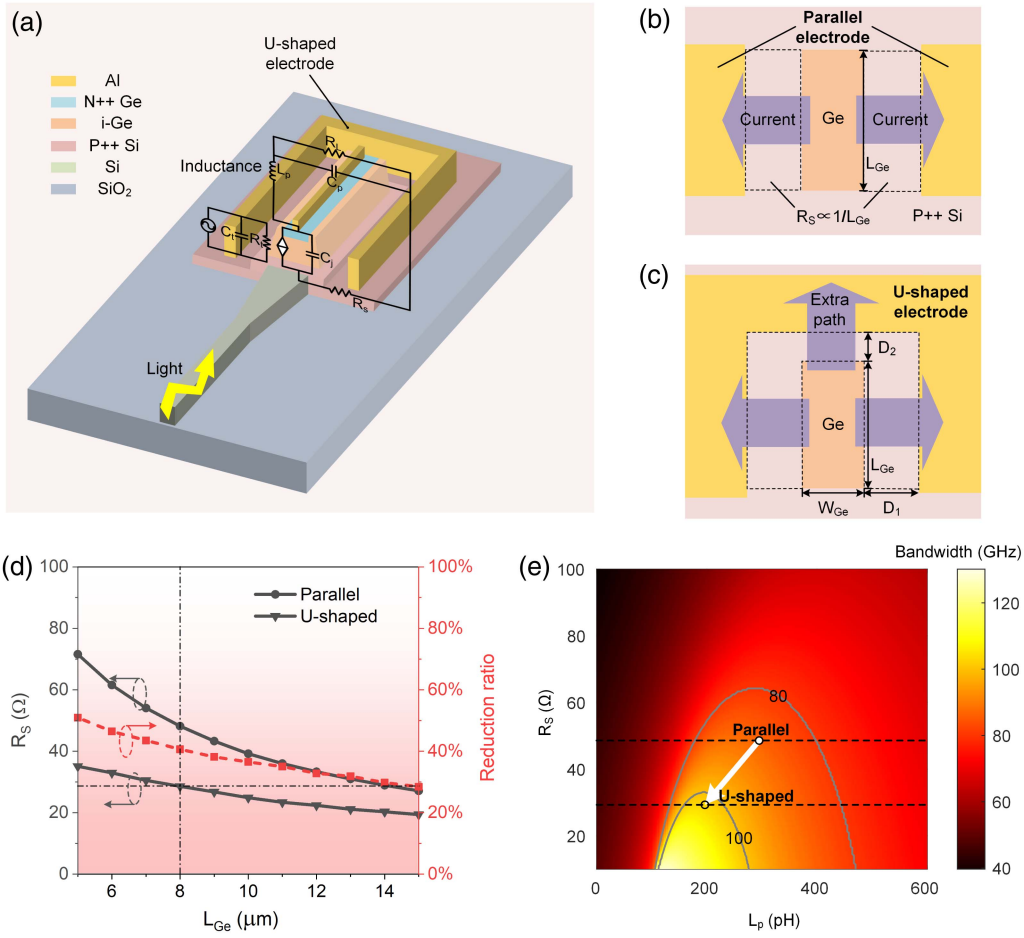

Fig. 1. (a) Structural schematic of the waveguide Ge PD with a U-shaped electrode. The cross section of the silicon waveguide is 500 nm × 220 nm and the silicon taper is 40 μm in length. Al, aluminum; Si, silicon; SiO_2, silica. The equivalent circuit is shown including the transit time and RC parasitic parameters. The transit time is represented by the equivalent resistance R_t and the equivalent capacitance C_t. The RC parasitic parameters contain the junction capacitance C_j, series resistance R_S, inductance L_p, and stray capacitance C_p as well as external load R_L. (b) The top view of the conventional waveguide Ge PD with the parallel electrode. The dashed region represents R_S. (c) The top view of the proposed PD with the U-shaped electrode. (d) The simulated R_S versus L_{Ge} under two kinds of contact and corresponding reduction ratio of the series resistance. Reduction ratio $= (R_{S,\text{Parallel}} - R_{S,\text{U-shaped}})/R_{S,\text{Parallel}} \times 100\%$. (e) The simulated bandwidth related to R_S and on-electrode inductance L_p when $C_j = 16$ fF.

proportional to the Ge area, i.e., Ge length when the width is fixed. R_S is a resistance perceived by the photocurrent flowing from the Ge region to the electrode, and thus it is inversely proportional to the collection cross section of the P^{++} silicon layer, i.e., Ge length when silicon thickness is fixed. As a result, the product of R_S and C_j is independent of the Ge length, and it is difficult to reduce R_S and C_j concurrently by solely tailoring the Ge geometry. We introduce a U-shaped electrode to alleviate this issue, as shown in Fig. 1(c). By connecting the metal electrodes on both sides of Ge, an extra carrier collection path is established, increasing the series resistance area (i.e., reducing R_S). Thanks to the unchanged Ge length, the junction capacitance is not increased. It should be noted that the perceived resistance along each of the three carrier collection paths must be equal. Otherwise, the photocurrent tends to concentrate on the path with the lowest resistance, resulting in the discount of previously indicated series resistance reduction strategy. To make it, the space between the Ge edge and the U-shaped electrode should match a design criterion, for a rectangular Ge region typically with unequal length and width:

$$\frac{D_1}{D_2} = \frac{W_{\mathrm{Ge}}}{L_{\mathrm{Ge}}}, \tag{1}$$

where W_{Ge} and L_{Ge} are the width and length of the Ge region, while D_1 and D_2 represent the gaps from the Ge length edge and width edge to the electrode, respectively. Under this condition, the simulated R_S versus L_{Ge} adopting two kinds of electrode is shown in Fig. 1(d). In both cases, R_S decreases inversely with Ge length, and it is reduced by 30%–50% under the U-shaped electrode compared with the parallel one. The L_{Ge} and W_{Ge} are selected to be 8 and 5 μm to ensure sufficient optical absorption at 1550 nm and a low junction capacitance (∼16 fF). Here, the Ge width of 5 μm is chosen by comprehensively considering the optical absorption and fabrication capability. If the fabrication process permits, an appropriate reduction of the Ge width can be expected to further reduce the junction capacitance C_j. Under this circumstance, R_S is reduced from 48 to 28 Ω with a ratio of 40.6%. If the parallel electrode is adopted, the Ge length needs to extend from 8 to 14 μm to achieve the same R_S decrease, while the junction capacitance is increased by 75%. Finally, D_1/D_2 needs to be 0.625, and $D_1 = 1.6$ μm and $D_2 = 2.56$ μm are selected.

We show that reducing the series resistance is important to the bandwidth. Figure 1(e) presents the simulated bandwidth related to R_S and on-electrode inductance L_p under $C_j = 16$ fF, using the equivalent circuit shown in Fig. 1(a). The gray solid lines denote the bandwidths of 80 and 100 GHz, and the black dashed lines represent the series resistances under parallel and U-shaped electrodes, respectively. It can be observed that when L_p is constant, the bandwidth increases as the R_S decreases. While R_S remains constant, the bandwidth first increases and subsequently decreases with L_p. Therefore, there is an optimal L_p to maximize the bandwidth. The bandwidth under the U-shaped electrode (with $L_{p,\mathrm{opt}} = 220$ pH) is increased from 87 to 110 GHz compared with the parallel electrode (with $L_{p,\mathrm{opt}} = 300$ pH). The 110 GHz bandwidth approaches the theoretical limit of the 350 nm intrinsic region.

3. EXPERIMENTAL RESULTS

To investigate the influence of using the U-shaped electrode, we fabricated two PDs with U-shaped and conventional parallel electrodes, respectively. The one with the U-shaped electrode is matched with a 220 pH inductance and the other with the parallel electrode adopts a 300 pH inductance. Figure 2(a) shows the cross-section diagram of the PDs along the length direction. The PDs are fabricated using a silicon-on-insulator wafer with a 220 nm thick silicon top layer and a 2 μm buried oxide layer. The silicon layer is etched into the ridge waveguide with a 90 nm slab. Then, the silicon top layer is P^{++} doped using boron of $\sim 10^{20}$ cm^{-3}. A 400 nm Ge is deposited on the doping region of the silicon, and ∼50 nm N^{++} doping of phosphorus is implanted on the top of the Ge to form the vertical n-i-p junction. The metals contacted to N^{++} Ge and P^{++} silicon are fabricated, and subsequently a second metal layer is fabricated to form different inductances. The two PDs are identical except for the silicon-contacted electrode and matching inductance. The microscope image of the fabricated PD with the U-shaped electrode is shown in Fig. 2(b). Here, a middle electrode with length of 195 μm and thickness of 2 μm is adopted for the desired 220 pH inductance. For the parallel one, the length is set as 245 μm for a 300 pH inductance. The detail of the red dashed region is shown in Fig. 2(c), and the Ge region and the U-shaped electrode are highlighted.

The current-voltage *(I-V)* characteristics of the two PDs are measured, as shown in Fig. 2(d). The photocurrent is measured at 1550 nm under a received optical power of −10 dBm, by extracting the coupling loss of 4.6 dB (denoted as α_c) according to a referenced grating coupler. The photocurrents and dark currents of the two PDs are similar under different bias voltages, indicating that the U-shaped electrode does not degrade the static performance. Very low dark currents of 1.3 and 1.9 nA are measured at −1 V for the U-shaped and parallel electrodes, respectively. Even at −4 V, the dark currents are lower than 7 nA. The good dark current performance is contributed by the robust fabrication process and compact Ge footprint. The photocurrent is almost constant under 0 to −4 V owing to the built-in electric field that is capable of sweeping out most of the photo-generated carriers within their lifetime. Then, we measure the photocurrent (I_{ph}) under different optical power input to the grating coupler (P_{in}). The $I_{\mathrm{ph}} \sim (\alpha_c P_{\mathrm{in}})$ relation is plotted and linearly fitted, where $\alpha_c P_{\mathrm{in}}$ represents the optical power fed into the PD by extracting the coupling loss. The slope of the fitted straight line is the measured optical responsivity. The measured photocurrents with different input optical power at −1 V are shown in Fig. 2(e), and the optical responsivities are 0.95 and 0.92 A/W for the U-shaped and parallel PDs, respectively. The former shows a slightly higher responsivity possibly due to higher carrier collection efficiency under a longer collection length [20].

Small-signal radio-frequency measurements are carried out using a 110 GHz light component analyzer (Keysight N4372E) in the test range of 10 MHz to 110 GHz. The Impedance Standard Substrate is used to calibrate the bias-tee, cables, and microprobe. The measured normalized S_{21} parameters are shown in Fig. 2(f). For the PD with the U-shaped electrode, the bandwidths are 13, 59, and 103 GHz under voltages of 0,

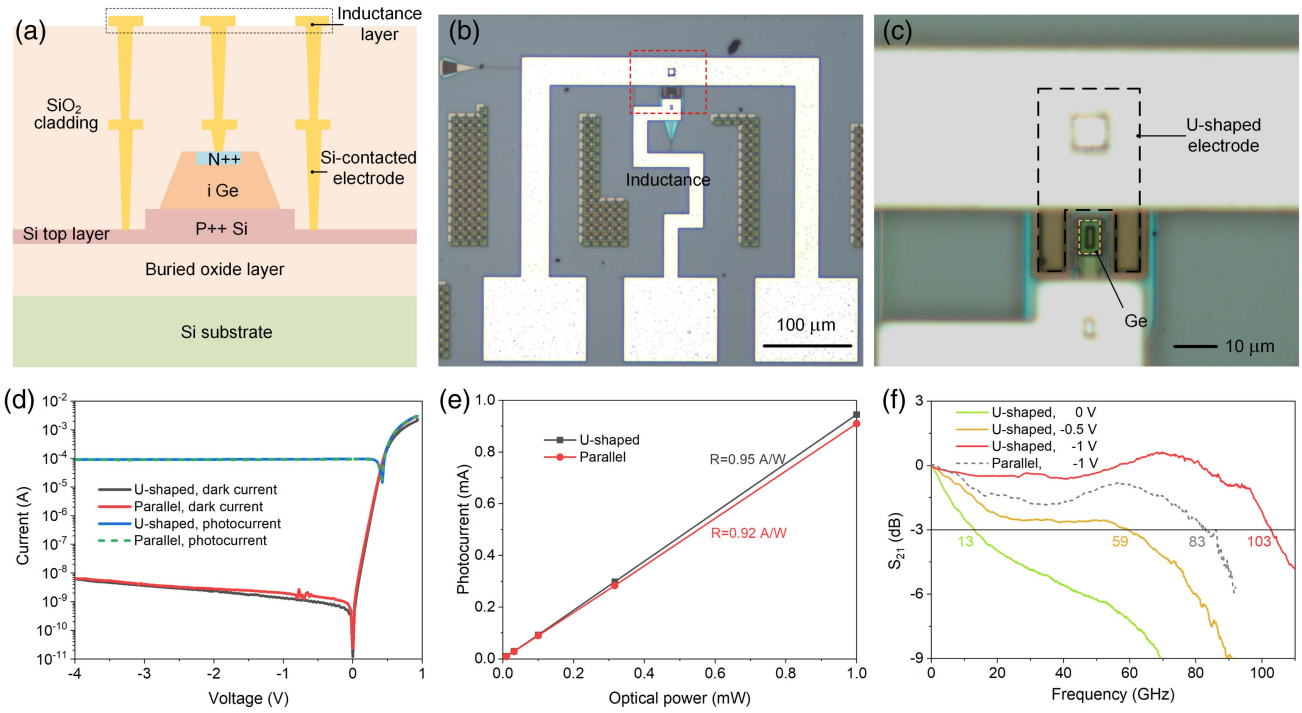

Fig. 2. (a) The cross-section diagram of the PDs along the length direction. Si, silicon. (b) The microscope images of the fabricated PD with the U-shaped electrode. (c) The enlarged view of the active region and U-shaped electrode. (d) The measures *I-V* characteristics of the two kinds of PDs. (e) The measured photocurrent with the input optical power at −1 V. (f) The measured normalized S_{21} parameters of the PDs with U-shaped and parallel electrodes.

−0.5, and −1 V, respectively. The relatively lower bandwidths at 0 and −0.5 V result from the slower carrier movement than the saturation velocity. The bandwidth reaches its maximum at −1 V and exceeds 100 GHz. Similarly, the maximum bandwidth of 83 GHz under the parallel situation is also obtained at −1 V, as shown in Fig. 2(f) for reference. We fit the measured S_{11} parameters using the equivalent circuit model from 10 MHz to 110 GHz and Table 1 shows the extracted parameters. The series resistance of the PD with the U-shaped electrode is 12.9 Ω, while the value is 20.1 Ω for the PD with the conventional parallel electrode. This indicates 36% reduced series resistance. The RC-limited bandwidth is also simulated to be 155 GHz, and thus the total bandwidth of 103 GHz is limited by the carrier transit time. These results indicate that the U-shaped electrode enables reducing series resistance and improving bandwidth.

The high-speed performance of the U-shaped PD is characterized via eye diagrams using a real-time digital storage oscilloscope with 256 GSa/s sampling rate (Keysight UXR0594AP). An OOK or PAM4 signal with a pattern length of $2^{15}-1$ is generated by an arbitrary waveform generator (Keysight M8199A) and amplified by a 45 GHz high-speed driver. A 40 GHz Mach–Zehnder modulator is adopted to modulate the continuous-wave light. The optical signal is fed into the fabricated PD and the resulting electrical signal is collected by the oscilloscope. The post-compensation and offline digital signal process is carried out to deduct the distortion of high-speed electrical signals through the cables and the transmitter [21,22]. As shown in Fig. 3, we measure the eye diagrams for 100, 112, and 120 Gb/s OOK signals by setting the input optical power as −4, −4, and −1 dBm. The signal-to-noise ratios (SNRs) are 14.76, 12.13, and 11.12 dB, respectively. Furthermore, the PD is used to receive 100, 112, and 200 Gb/s PAM4 signals, under the input optical power of −4, −4, and −1 dBm. The SNRs are 25.39, 23.89, and 19.44 dB, respectively. These results make the proposed PD very

Table 1. Extracted Parameters of the Electrical Elements

Device	C_j (fF)	R_S (Ω)	L_p (pH)	C_p (fF)	R_L (Ω)
U-shaped	22.6	12.9	175.3	10.0	50
Parallel	24.0	20.1	217.3	10.3	50

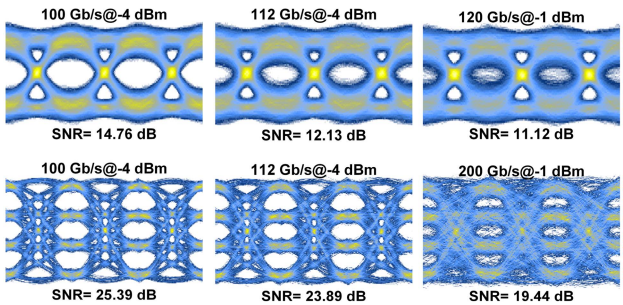

Fig. 3. Measured eye diagrams for 100/112/120 Gb/s OOK signals and 100/112/200 Gb/s PAM4 signals at −1 V.

Table 2. Literature Overview of the State-of-the-Art High-Speed Waveguide PDs Integrated on Silicon[a]

Ref.	Type	Voltage (V)	R (A/W)	I_D (nA)	BW (GHz)	RBP ($A \cdot W^{-1} \cdot GHz$)	D^* ($cm \cdot Hz^{1/2} \cdot W^{-1}$)
[23]	InP/InGaAs	−2	0.2	0.12	70	14	1.61×10^9
[24]	$MoTe_2$	−3	0.2	10–1000	24	4.8	$\sim 1.22 \times 10^9$
[25]	Graphene	−0.3	0.4	–	>40	~16	$\sim 1.5 \times 10^9$
[26]	Ge, lateral	−1	1.0	100	70	70	1.77×10^9
[27]	Ge, lateral	−1	0.74	2.5	67	50	6.78×10^9
[14]	Ge, lateral	−2	0.3	<200	265	79.5	$\sim 2.37 \times 10^8$
			0.45	<100	240	108	$\sim 5.03 \times 10^8$
[19]	Ge, vertical	−3	0.89	6.4	80	71.2	1.33×10^{10}
[21]	Ge, vertical	−2	1.05	6.4	67	70	1.44×10^{10}
[18]	Ge, vertical	−3	0.81	35	75	61	4.84×10^9
This work	**Ge, vertical**	**−1**	**0.95**	**1.3**	**103**	**98**	$\mathbf{2.95 \times 10^{10}}$

[a] R, responsivity; I_D, dark current; BW, bandwidth; RBP, responsivity-bandwidth product; D^*, specific detectivity.

competitive to satisfy the demands in the application with large-capacity data transmissions.

4. DISCUSSION

Table 2 presents the literature overview of the state-of-the-art high-speed silicon-based PDs. InP and two-dimensional material PDs achieve bandwidths of several tens of gigahertz, while the optical responsivities are typically low due to the weak optical coupling and light–matter interaction [23–25]. They also suffer from relatively complex fabrication. The waveguide Ge PDs benefit from CMOS-compatible fabrication, and they can be divided into vertical and lateral types according to the spatial distribution direction of the p-i-n junction. The lateral Ge PDs are practically easier to achieve narrow intrinsic regions and thus larger bandwidths. For instance, Ref. [14] achieves an ultra-high bandwidth up to 265 GHz through a 100 nm intrinsic region. However, the responsivity and dark current inevitably deteriorate. Furthermore, a more complex process is required, including chemical mechanical polishing and Ge corrosion. The vertical Ge PDs are more popular due to the simple fabrication process and robust manufacturing. However, the bandwidth improvement has become even more difficult due to relatively larger volume, and previous works exhibit responsivities of 0.8–1 A/W and bandwidths of 67–80 GHz. This work is the first vertical Ge PD with a bandwidth greater than 100 GHz. We attribute this result to the optimized parasitic parameters comprehensively regulated by the U-shaped electrode and on-electrode inductance. Meanwhile, thanks to the high responsivity, the responsivity-bandwidth product of 98 $A \cdot W^{-1} \cdot GHz$ is also the highest result among the vertical PDs.

For data communication, responsivity and dark current comprehensively determine the sensitivity of the optical receiver, which is crucial for reducing power consumption, relaxing the requirement of high-power lasers, and suppressing optical nonlinearity. The specific detectivity (D^*) is used to evaluate the sensitivity, taking into account both responsivity and dark current [28,29]. This work has reached the highest specific detectivity of 2.95×10^{10} $cm \cdot Hz^{1/2} \cdot W^{-1}$ among these Ge PDs due to ultra-low dark current. Although Ref. [21] has a higher responsivity, it has ~5× higher dark current, therefore having a slightly lower D^*. Overall, this work provides a simple-fabrication, high-speed, and highly sensitive PD for the SiPICs and optical interconnects.

In addition to the Ge PIN PD, the SiGe avalanche photodiode (APD) is also important for optical interconnects, and it typically provides 5–10 dB higher sensitivity due to the internal gain by applying a high voltage to provide a strong electric field in the intrinsic Si region for impact ionization [30]. Several investigations suggested a thin intrinsic Si [31] or PIN structure with Ge multiplication [32] to reduce the bias voltage. On the other hand, the bandwidths of SiGe APDs are typically lower than that of the PIN PDs, and schemes with thin intrinsic region [31] and resonance effect [33] were demonstrated to improve the bandwidth.

5. CONCLUSION

In conclusion, we demonstrate that the optimal U-shaped electrode can improve PD bandwidth compared with the conventional PD. At −1 V, the measured 3 dB bandwidth is 103 GHz, together with high responsivity and ultra-low dark current. High-speed optical reception based on the proposed PD is demonstrated with 120 Gb/s OOK and 200 Gb/s PAM4 signals. This work may pave the way for chip-based optical receivers in ultra-high-speed optical interconnects.

Funding. National Key Research and Development Program of China (2019YFB1803801); National Natural Science Foundation of China (61922034, 62135004); Key Research and Development Program of Hubei Province (2021BAA005); Innovation Project of Optics Valley Laboratory (OVL2021BG005); Program for HUST Academic Frontier Youth Team (2018QYTD08).

Disclosures. The authors declare no conflicts of interest.

Data Availability. The data that support the findings of this study are available from the authors upon reasonable request.

REFERENCES

1. H. Shu, L. Chang, and Y. Tao, *et al.*, "Microcomb-driven silicon photonic systems," Nature **605**, 457–463 (2022).
2. C. Sun, M. T. Wade, and Y. Lee, *et al.*, "Single-chip microprocessor that communicates directly using light," Nature **528**, 534–538 (2015).

3. X. Qiang, X. Zhou, and J. Wang, *et al.*, "Large-scale silicon quantum photonics implementing arbitrary two-qubit processing," Nat. Photonics **12**, 534–539 (2018).
4. P. Dong, Y.-K. Chen, and G.-H. Duan, *et al.*, "Silicon photonic devices and integrated circuits," Nanophotonics **3**, 215–228 (2014).
5. Y. Shi, Y. Zhang, and Y. Wan, *et al.*, "Silicon photonics for high-capacity data communications," Photonics Res. **10**, A106–A134 (2022).
6. H. Chen, C. Jin, and B. Huang, *et al.*, "Integrated cladding-pumped multicore few-mode erbium-doped fibre amplifier for space-division-multiplexed communications," Nat. Photonics **10**, 529–533 (2016).
7. G. Rademacher, B. J. Puttnam, and R. S. Luís, *et al.*, "Peta-bit-per-second optical communications system using a standard cladding diameter 15-mode fiber," Nat. Commun. **12**, 4238 (2021).
8. A. Beling, H.-G. Bach, and G. G. Mekonnen, *et al.*, "High-speed miniaturized photodiode and parallel-fed traveling-wave photodetectors based on InP," IEEE J. Sel. Top. Quantum Electron. **13**, 15–21 (2007).
9. E. Rouvalis, M. Chtioui, and F. Van Dijk, *et al.*, "170 GHz uni-traveling carrier photodiodes for InP-based photonic integrated circuits," Opt. Express **20**, 20090–20095 (2012).
10. P. Ma, Y. Salamin, and B. Baeuerle, *et al.*, "Plasmonically enhanced graphene photodetector featuring 100 Gbit/s data reception, high responsivity, and compact size," ACS Photonics **6**, 154–161 (2018).
11. S. M. Koepfli, M. Eppenberger, and M. S.-B. Hossain, *et al.*, ">500 GHz bandwidth graphene photodetector enabling highest-capacity plasmonic-to-plasmonic links," in *European Conference on Optical Communication (ECOC)* (2022), pp. 1–4.
12. L. Vivien, A. Polzer, and D. Marris-Morini, *et al.*, "Zero-bias 40 Gbit/s germanium waveguide photodetector on silicon," Opt. Express **20**, 1096–1101 (2012).
13. S. Lischke, A. Peczek, and F. Korndörfer, *et al.*, "Ge photodiode with −3 dB OE bandwidth of 110 GHz for PIC and ePIC platforms," in *IEEE International Electron Devices Meeting (IEDM)* (2020), pp. 7.3.1–7.3.4.
14. S. Lischke, A. Peczek, and J. Morgan, *et al.*, "Ultra-fast germanium photodiode with 3-dB bandwidth of 265 GHz," Nat. Photonics **15**, 925–931 (2021).
15. Z. Liu, C. Li, and B. Cheng, "A new 3-dB bandwidth record of Ge photodiode on Si," J. Semicond. **43**, 060202 (2022).
16. M. Gould, T. Baehr-Jones, and R. Ding, *et al.*, "Bandwidth enhancement of waveguide-coupled photodetectors with inductive gain peaking," Opt. Express **20**, 7101–7111 (2012).
17. G. Chen, Y. Yu, and S. Deng, *et al.*, "Bandwidth improvement for germanium photodetector using wire bonding technology," Opt. Express **23**, 25700–25706 (2015).
18. X. Li, Y. Zhu, and Z. Liu, *et al.*, "75 GHz germanium waveguide photodetector with 64 Gbps data rates utilizing an inductive-gain-peaking technique," J. Semicond. **44**, 012301 (2023).
19. Y. Shi, D. Zhou, and Y. Yu, *et al.*, "80 GHz germanium waveguide photodiode enabled by parasitic parameter engineering," Photonics Res. **9**, 605–609 (2021).
20. L. Li, L. Jin, and Y. Zhou, *et al.*, "Filterless polarization-sensitive 2D perovskite narrowband photodetectors," Adv. Opt. Mater. **7**, 1900988 (2019).
21. D. Chen, H. Zhang, and M. Liu, *et al.*, "67 GHz light-trapping-structure germanium photodetector supporting 240 Gb/s PAM-4 transmission," Photonics Res. **10**, 2165–2171 (2022).
22. Y. Xiang, H. Cao, and C. Liu, *et al.*, "High-speed waveguide Ge/Si avalanche photodiode with a gain-bandwidth product of 615 GHz," Optica **9**, 762–769 (2022).
23. P. Wen, P. Tiwari, and S. Mauthe, *et al.*, "Waveguide coupled III-V photodiodes monolithically integrated on Si," Nat. Commun. **13**, 909 (2022).
24. N. Flöry, P. Ma, and Y. Salamin, *et al.*, "Waveguide-integrated van der Waals heterostructure photodetector at telecom wavelengths with high speed and high responsivity," Nat. Nanotechnol. **15**, 118–124 (2020).
25. J. Guo, J. Li, and C. Liu, *et al.*, "High-performance silicon-graphene hybrid plasmonic waveguide photodetectors beyond 1.55 μm," Light Sci. Appl. **9**, 29 (2020).
26. S. Lischke, D. Knoll, and C. Mai, *et al.*, "High bandwidth, high responsivity waveguide-coupled germanium pin photodiode," Opt. Express **23**, 27213–27220 (2015).
27. H. Chen, P. Verheyen, and P. De Heyn, *et al.*, "−1 V bias 67 GHz bandwidth Si-contacted germanium waveguide pin photodetector for optical links at 56 Gbps and beyond," Opt. Express **24**, 4622–4631 (2016).
28. Y. Lin, K. H. Lee, and B. Son, *et al.*, "Low-power and high-detectivity Ge photodiodes by *in-situ* heavy As doping during Ge-on-Si seed layer growth," Opt. Express **29**, 2940–2952 (2021).
29. G. Chen, Y. Yu, and Y. Shi, *et al.*, "High-speed photodetectors on silicon photonics platform for optical interconnect," Laser Photonics Rev. **16**, 2200117 (2022).
30. Y. Kang, H.-D. Liu, and M. Morse, *et al.*, "Monolithic germanium/silicon avalanche photodiodes with 340 GHz gain-bandwidth product," Nat. Photonics **3**, 59–63 (2009).
31. Z. Huang, C. Li, and D. Liang, *et al.*, "25 Gbps low-voltage waveguide Si-Ge avalanche photodiode," Optica **3**, 793–798 (2016).
32. D. Benedikovic, L. Virot, and G. Aubin, *et al.*, "40 Gbps heterostructure germanium avalanche photo receiver on a silicon chip," Optica **7**, 775–783 (2020).
33. B. Wang and J. Mu, "High-speed Si-Ge avalanche photodiodes," PhotoniX **3**, 8 (2022).